Structure and Properties of the $Mo_3Nb_2O_{14}$ Oxide

Pavel Afanasiev*

Institut de Recherches sur la Catalyze 2, Avenue A. Einstein, 69626 Villeurbanne Cédex, France

Received: February 1, 2005; In Final Form: June 22, 2005

Mixed Nb−Mo oxides were prepared by solid-state reaction of Nb(V) and Mo(VI) oxides at 973−1123 K. Optimal conditions were determined for the formation of the $Mo_3Nb_2O_{14}$ compound. As established by Rietveld refinement of the powder X-ray diffraction patterns, the $Mo_3Nb_2O_{14}$ oxide has the tetragonal cell with $a = 23.150(6)$ Å and $c = 3.998(4)$ Å and a tunnel structure similar to that of the Mo_5O_{14} oxide. The solids were characterized by several physical techniques, including scanning and transmission electron microscopy, FT-IR, UV−visible diffuse reflectance spectroscopy, X-ray photoelectron spectroscopy, and electron spin resonance spectroscopy. It has been shown that the $Mo_3Nb_2O_{14}$ solid prepared in air at 973−1073 K after cooling to room temperature contains high amounts of Mo(V) species (ca. 1% of total molybdenum). The presence of paramagnetic species correlates with the intense green color of the solids and the strong d−d transition band in the UV−visible spectra, typical for the d^1 species. The amount of paramagnetic species does not depend on the solid annealing and/or on the small variations of its composition. Neither is it related to the oxygen release upon the solid heating, being therefore an intrinsic property of the $Mo_3Nb_2O_{14}$ oxide. The unusual stabilization of reduced Mo species in the highly oxidizing conditions was explained by the substitution disorder between Nb and Mo atoms. It is supposed that a configuration containing μ_3 oxygen bonded to three Mo(VI) atoms is unstable and decomposes, leading to a Mo(V) center and a hole in the valence band.

Introduction

Mixed oxides of IV−VI transition metals are important inorganic materials used in diverse fields such as catalysis, ceramics, and microelectronics. Complex oxide formulations including Nb and Mo are extensively used in partial oxidation catalysis.[1,2]

Earlier we prepared the Nb−Mo mixed oxides as the precursors for further synthesis of the mixed sulfide catalysts.[3] In the meantime we observed that the oxide of composition $Nb_2O_5 \cdot 3MoO_3$ has unexpected intense green coloration. Both Nb(V) and Mo(VI) oxides are d^0 compounds and are white or slightly colored; their charge-transfer bands are localized in the 200−400 nm region. For a solid obtained by means of firing in air at 1123 K of a mixture of two d^0 oxides, the intense green color seemed unusual, because it suggested the appearance of a d−d transition and therefore some reduction. Another possible explanation of the finding was the formation of a new low-symmetry crystalline structure, in which the charge-transfer band is strongly shifted to the lower wavelengths region.

When trying to identify the obtained Nb−Mo oxide using powder X-ray diffraction (XRD), we noticed that for this oxide the XRD literature data are confusing. The Nb−Mo mixed oxides are poorly studied. Indeed, in the 2004 update of the ICDS inorganic crystal structures database,[4] nothing can be found for the Nb−Mo oxides, in contrast to the homologous oxide systems W−Nb (11 entries) and W−Ta (7 entries). The goal of the present work is to clarify the structure and to explain the properties of the $Mo_3Nb_2O_{14}$ oxide.

Experimental Section

The mixed oxides were prepared using high purity grade precursors from Aldrich. Thoroughly ground mixtures of MoO_3 (99.8%) and Nb_2O_5 (99.9%) were heated in air in ceramic crucibles or in quartz ampules sealed under evacuation, for 12 h in the temperature range of 973−1173 K.

TABLE 1: Solids Prepared (Preparation Conditions and the Results of Chemical Analysis and Powder XRD Phase Analysis)

sample name	initial reacn mixture composition	*T* prep, K	Nb/Mo in the product, data from chem anal	phases XRD
NbMo01	$3.02MoO_3 \cdot Nb_2O_5$	1123	6.25	$MoNb_6O_{18}$
NbMo02	$3.00MoO_3 \cdot Nb_2O_5$	1123	6.98	$MoNb_6O_{18}$
NbMo03	$2.98MoO_3 \cdot Nb_2O_5$	1123	5.38	$MoNb_6O_{18}$
NbMo04	$0.30\ MoO_3.Nb_2O_5$[a]	1173	*b*	MoO_3, $MoNb_6O_{18}$
NbMo05	$0.30\ MoO_3 \cdot Nb_2O_5$	1173		Nb_2O_5
NbMo06	$3.00MoO_3 \cdot Nb_2O_5$[a]	1173		MoO_3 $MoNb_6O_{18}$
NbMo07	$3.00MoO_3 \cdot Nb_2O_5$	1023	0.737	$Mo_3Nb_2O_{14}$ $MoNb_6O_{18}$[c]
NbMo08	$3.02MoO_3 \cdot Nb_2O_5$	1023	0.706	$Mo_3Nb_2O_{14}$ $MoNb_6O_{18}$[c]
NbMo09	$2.98MoO_3 \cdot Nb_2O_5$	1023	0.794	$Mo_3Nb_2O_{14}$ $MoNb_6O_{18}$[c]
NbMo10	$3.00MoO_3 \cdot Nb_2O_5$	973	0.666	$Mo_3Nb_2O_{14}$
NbMo11	$6.00MoO_3 \cdot Nb_2O_5$	973		MoO_3, $Mo_3Nb_2O_{14}$

[a] Prepared in the sealed quartz ampules; otherwise prepared in open air. [b] Not determined. [c] Small impurity.

To verify whether the properties of the solids obtained are preparation-dependent, the quenching conditions and the amounts of the oxides loaded were varied from slow exponential cooling in the furnace to immediate immersion of hot samples into liquid nitrogen. The composition of the initial mixtures was slightly varied (Table 1) in order to verify the eventual effects of small deviations from the stoichiometry on the properties of the solid products.

The X-ray diffraction patterns were obtained on a Bruker D5005 diffractometer with Cu Kα emission. The diffractograms were analyzed using the standard JCPDS files. Rietveld refinement of the oxide structure was carried out using the Fullprof

* To whom correspondence should be addressed. Telephone: 33 4 7244 53 39. Fax: 33 4 72 44 53 99. E-mail: afanas@catalyse.univ-lyon1.fr.

10.1021/jp050554u CCC: $30.25
Published on Web 09/13/2005

program (FullProf.2k version)[5] and verified with the same input data using the refinement facility of the Powdercell 2.3 program.[6] Indexation of the unit cell was carried out using TREOR97[7] and DICVOL04[8] programs. The convergence of the results from different packages has been tested in order to provide better reliability of the refinement. The diffractograms for the Rietveld refinement were measured with the 2θ step of 0.01° and the accumulation time of 8 s/point. For precise positions of the diffraction peaks, the XRD patterns were detected additionally for the specimens mixed with a silicon 640c National Institute of Standards and Technology (NIST) standard. The background function was subtracted using a cubic spline. The instrumental broadening function was independently obtained using a pattern of well-crystallized substance with isotropic particles (NaCl). An absorption correction was not needed because of the flat sample geometry. After the $K_{\alpha 2}$ stripping and high-frequency Fourier smoothing the diffraction peaks shape was examined for several selected peaks using PEAKFIT software (Jandel Corp.).

Chemical analyses were realized using the atomic emission method on a AES−ICP Spectroflame-ICP, model D spectrometer. Prior to analysis, the solids were dissolved in HF acid. The ESR spectra were registered at variable temperatures from 77 to 540 K using a Varian E9 spectrometer working in the X band. The g values were measured relative to the Diphenyl Pircyl Hydrazyl (DPPH) reference ($g = 2.0036$). Radiowave power applied was always below the saturation level, so that we could estimate the total number of the unpaired electrons. Calculation of the number of paramagnetic centers was performed by double integration of the spectra normalized to the of Varian strong pitch sample ($g = 2.0028$, 3×10^{15} spins·cm^{-1}). UV−visible diffuse reflectance spectra were measured on a Perkin-Elmer lambda 9 spectrometer, using as a reference MgO standard. The edge energy from the UV−visible diffuse reflectance spectra was calculated according to ref 9. X-ray photoelectron spectroscopy (XPS) studies were performed on a VG ESCALAB 200R spectrometer using Al Kα radiation. The XPS spectra of O 1s, Nb 3d, and Mo 3d were recorded and their binding energies (BE) referred to the energy of the C 1s peak (BE = 285.0 eV). For measurement, the samples were pressed into indium foil. The charging effect on insulated oxides under study was compensated for by using an electron gun. The quality vacuum in the analysis chamber was better than 10^{-7} Pa. Deconvolution of XPS peaks and quantification of the surface contents of the elements was done using the sensitivity factors provided with the VG software. IR spectra were measured in transmission mode in KBr disks in air on a Bruker Vector 22 device. To make a pellet, a weighted amount (ca 3 mg) of the sample was mixed with 200 mg of KBr. Scanning electron microscopy images were obtained on a Hitachi S800 device at the CMEABG center of the Lyon Claude Bernard University, at the accelerating voltage of 25 kV. The solids were covered with Pd−Au alloy prior to measurement in order to avoid charging with the electron beam. Transmission electron micrographs were obtained on a JEOL 2010 electron microscope with a LaB_6 filament as the source of electrons, operated at 200 kV. Samples were mounted on a microgrid carbon polymer supported on a copper grid by placing a few droplets of a suspension of ground sample in ethanol on the grid, followed by drying at ambient conditions. Energy dispersive analysis system (Link Isis) with diode allowing detection of light elements ($Z > 5$) was applied. The gaseous products evolved upon heating of the oxide mixtures were studied using a mass spectrometer gas trace A (Fison Instruments) equipped with a quadrupole analyzer working in Faraday mode. The oxide mixtures (ca. 2 g) were heated from room temperature to 1000 °C in a quarz cell at the heating rate of 5 K min^{-1}. A silica capillary tube heated at 453 K continuously bled off a proportion of the gaseous reaction products. Several signals were registered, those with $m/e = 16$, 17, 18, 32, and 46, corresponding respectively to the ionized species of H_2O, O_2, CO_2, and their fragments.

Results and Discussion

The reaction conditions and the composition of the products obtained are summarized in Table 1. The target phase $Mo_3Nb_2O_{14}$ was identified in the samples NbMo7−NbMo10 prepared at 973−1073 K. From the data of Table 1, it follows that if the reaction is carried out at high temperatures in open ceramic crucibles, the amount of molybdenum in the solids obtained is much lower than in the initial reaction mixtures, due to the volatility of the molybdenum oxide. For the reaction temperatures higher than 1023 K the target mixed oxide cannot be formed in open air since it decomposes to MoO_3 and another Nb−Mo oxide with lower Mo content, further designated as "$MoNb_6O_{18}$ phase". Carrying out the reaction in sealed quartz ampules does not resolve the problem since decomposition still occurs but large crystals of MoO_3 are now present in the reaction products. Although this work is mostly focused on the $Mo_3Nb_2O_{14}$ oxide, the light violet−gray samples of the "$MoNb_6O_{18}$ phase" obtained at 1123 K (NbMo01−NbMo03) were retained for further study, and are discussed when relevant, for comparison of some physical properties.

The low-temperature limit at which $Mo_3Nb_2O_{14}$ formation occurs in a reasonable time corresponds to approximately 973 K. Thus, at 873 K the reaction rate is insufficient and the initial oxides are found in the products even after several days of reaction. Therefore for the oxide−oxide reaction, the temperature in a rather narrow interval 973−1023 K should be applied to obtain $Mo_3Nb_2O_{14}$ oxide. Other chemical routes to this oxide (sol−gel, molten salts, and so on) might off course be envisaged, but their study is beyond the scope of the present work.

Although we do not discuss here the $MoO_3-Nb_2O_5$ phase diagram, it is worth noting that the $Mo_3Nb_2O_{14}$ solid seems to be the richest in molybdenum among the individual Nb−Mo oxides available from the conventional solid-state reaction. Indeed, the experiments with the reaction mixtures containing a large excess of MoO_3 did not show any new phases but only the mixtures of $Mo_3Nb_2O_{14}$ and unreacted MoO_3.

While prepared in open air or in sealed ampules, all the solids containing the $Mo_3Nb_2O_{14}$ phase have similar intense green color. At the same time the total stoichiometry, as calculated from the chemical analysis data (Table 1), suggests that within the accuracy limits of the method all the solids should be d^0 oxides. The amount of reduced species (if any) corresponds to the slight deviations from the $Mo_3Nb_2O_{14}$ composition within the limits of the analysis accuracy (less than 1% of oxygen atoms).

Scanning electron microscopy shows that the solids obtained at 973−1123 K in open ceramic crucibles are homogeneous and consist of needlelike crystals of several micrometers in size (exemplified by NbMo10, Figure 1a). Transmission microscopy coupled with energy-dispersive spectrometry (EDS) shows nearly perfect homogeneity of the solid NbMo10 (Nb/Mo atomic ratio of 0.66), which is crystalline everywhere and gives good atomic resolution images and SAED patterns with the spots well corresponding to the XRD data (Figure 2b).

Though the "$Mo_3Nb_2O_{14}$" and "$MoNb_6O_{18}$" phases are mentioned in Table 1, here these formulas serve merely as

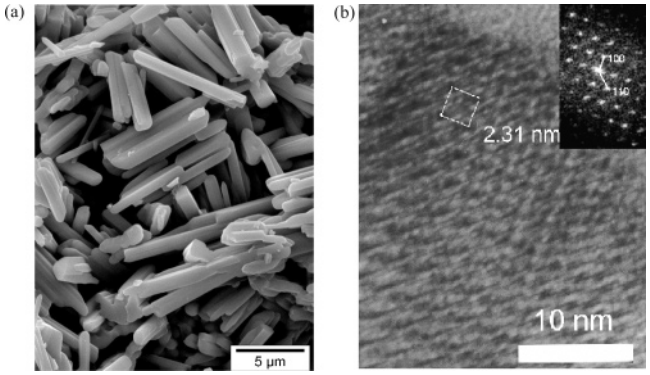

Figure 1. SEM micrograph of the $Mo_3Nb_2O_{14}$ solid, NbMo10 specimen (a) and HRTEM image of the same solid showing the lattice periodicity perpendicular to the *c* axis with (100) and (110) vectors of reciprocal lattice marked on the diffractogram (b).

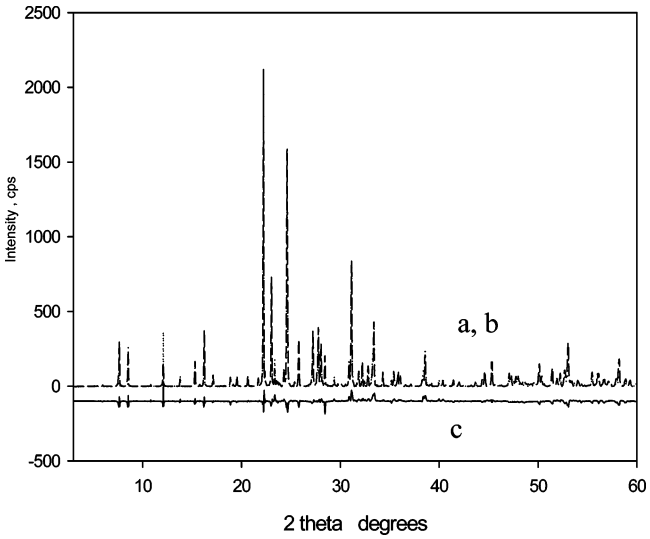

Figure 2. Rietveld refinement of the $Mo_3Nb_2O_{14}$ XRD pattern (specimen NbMo10): experimental data after background and $K_{\alpha 2}$ removal (a), calculated (b), and difference curve (c).

designations of the fingerprint XRD patterns of some unknown structures. In the JCPDS powder diffraction database (2004 updated), only two Nb−Mo mixed oxides can be found, one is $Nb_{0.09}Mo_{0.91}O_{2.8}$ (27-1310 card) and another one is named "$3MoO_2.Nb_2O_5$ oxide" ("deleted" quality card 18-0840). Both oxides have the line positions and intensities very similar to those of the binary $MoO_{2.8}$ (or Mo_5O_{14}) oxide, JCPDS card 12-0517. We suggested earlier in ref 3 that an error occurred in the JCPDS file 18-0840.

The violet-gray $MoNb_6O_{18}$ phase from the NbMo01−NbMo03 solids was indexed as having a tetragonal lattice cell with $a = 14.827$ Å and $c = 5.752$ Å. The structure of this solid will be published elsewhere. The $MoNb_6O_{18}$ is a single-phase ingenious Nb−Mo−O compound, demonstrating some "strange" properties, similarly to the $Mo_3Nb_2O_{14}$ solid, but containing much less molybdenum than the last.

For the Rietveld refinement of the $Mo_3Nb_2O_{14}$ structure, the sample NbMo10 was selected, with the chemical composition close to the ideal stoichiometry. Indexing of the XRD pattern for the NbMo10 solid using DICVOL and TREOR programs gives a tetragonal lattice cell, $a = 23.150(6)$ Å and $c = 3.998(4)$ Å. The Voight and Pearson VII profile functions provided the best fit quality ($r^2 = 0.996$ for a non-overlapping with other reflections stand alone line (630), having relative intensity 10

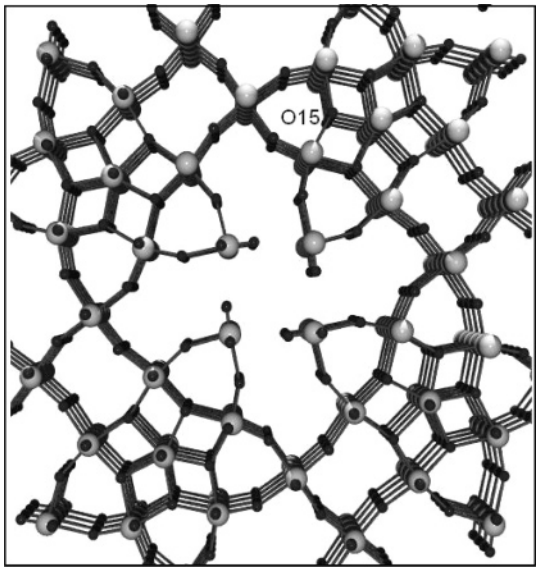

Figure 3. Crystal structure of the Mo_5O_{14} oxide along the (001) axis. Black spheres, oxygen; large gray circles, Nb or Mo. The O15 atom is marked.

at $d = 3.4499$). A slight asymmetry of peaks is observed for small diffraction angles.

Prior to refinement, an adequate structural model should be chosen. Among the known molybdenum and niobium oxides, the pattern of the Mo_5O_{14} compound appeared to give the best visual correspondence with the XRD pattern of $Mo_3Nb_2O_{14}$. The profile refinements of the XRD patterns were therefore performed in the *P4*/*mbm* (127) space group. The Mo_5O_{14} structure (Figure 3) is built up by MoO_6 polyhedra and MoO_7 pentagonal bipyramids connected by corners and edges.[10] Each pentagonal bipyramid shares its edges with five MoO_6 polyhedra. There are 22 atoms in this cell, and the relative occupancies of sites with Nb and Mo are not known. The similarity of Nb and Mo masses makes the simulated pattern only moderately sensible to the variations of the sites occupancy with Nb or Mo. Manual simulation of the XRD patterns with the Powdercell program showed that replacing Mo atoms in the Mo_5O_{14} structure with Nb, if carried out in an ordered manner, might slightly influence the relative intensities in the calculated patterns. However, the Rietveld algorithm cannot handle the task of finding the right configurations. Therefore it can be only postulated that the oxide adopts the Mo_5O_{14} structure without distinguishing the Mo and Nb positions. In any case, considering of Nb and Mo positional disorder is not necessary to achieve a good fit. A low weighted R_{wp} (7.33%) value might already be obtained by refining the global parameters and cell dimensions for the initial Mo_5O_{14} structure (ICSD 27202), adjusting the B_{iso} values but without refining of fractional atomic coordinates. Two-dimensional ordering as reported by Kihlborg for Mo_5O_{14} [10] was not observed in this solid; i.e., neither the supercell reflections were seen in the diffraction experiments nor the consideration of nonrandom sites occupation along *z*-axis was necessary to obtain a good Rietveld fit. The experimental and calculated patterns are depicted in Figure 2. Though satisfactory fit is obtained, the structural characterization cannot be considered as complete since Nb−Mo preferential occupation might still exist (not necessarily noticeably influencing the XRD patterns). To verify whether there is preferential occupation of sites in this structure, an EXAFS study will be desirable.

Earlier, Kihlborg, who reported on the structure of the reduced Mo_5O_{14} oxide, found that the binary oxide is metastable and

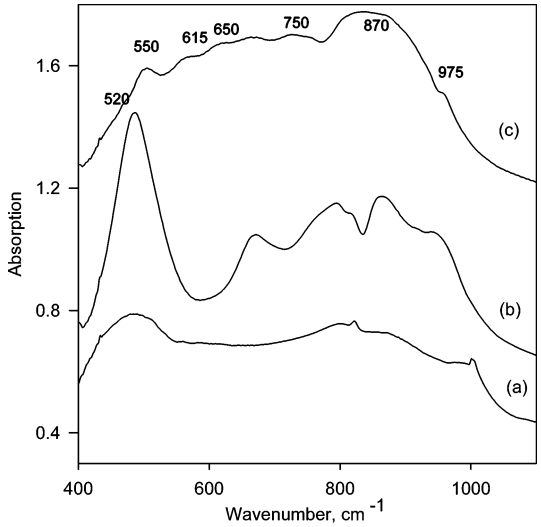

Figure 4. IR spectra of MoO_3 (a), Nb_2O_5 (b), and $Mo_3Nb_2O_{14}$ (c).

exists in the narrow temperature range near 500 °C.[10] However, it was noticed that the admixtures of Nb, Ta, and Ti increase its stability.[11] When such admixtures are introduced, the total M_5O_{14} stoichiometry is preserved (M = Nb, Mo, Ta, Ti). In the doped oxides; V and IV group transition metals preserve their highest oxidation degrees, whereas the formal oxidation degree of Mo somewhat increases. In the limiting case of $3MoO_3 \cdot Nb_2O_5$ the mixed oxide still has the M_5O_{14} stoichiometry, while both metals formally adopt the highest oxidation states.

The eminent importance of the Mo_5O_{14} structure for the catalytic properties of mixed oxides in partial oxidation has been suggested in several recent works. However, the solids possessing this structure are difficult to obtain in pure state or they correspond to the nonstoichiometric solid solutions. Here we describe a stoichiometric and thermally stable solid possessing the target Mo_5O_{14} structure. Thermal stability of this phase would allow preparing it in a highly dispersed state, appropriate for catalytic applications. It might be potentially interesting as a catalyst itself, but particularly as a generic host which might form a wide variety of solid solutions keeping the same Mo_5O_{14} tunnel structure.

The goal of this work was not only to clarify the structure of the mixed oxide but to give insight to its properties and particularly to its intense green color, which seemed unusual and thus initiated this study. The following sections discuss the results of physical characterizations, aimed to shed some light on this finding.

The IR spectra of the starting oxides and the mixed one are shown in Figure 4. The comparison of band maxima and shape suggests that transversal−longitudinal splitting, which is found in the molybdenum oxide (small sharp maxima at 820 and 100 cm^{-1}) due to its lamellar structure, is not present in the $Mo_3Nb_2O_{14}$. This is in agreement with Kihlborg's conclusion on the Mo_5O_{14} structure: though having a strongly anisotropic elementary cell, this mixed oxide is not a lamellar but a three-dimensional structure. In the infrared spectrum many features are obviously overlapped, but several maxima and shoulders can be clearly distinguished (cm^{-1}): 975 sh, 870 s, 750 m, 660 m, 620 m, 550 m, 520 sh.

High-frequency lines are due to the Mo═O double bond stretching, whereas the intense line at 750 cm^{-1} can be attributed to the Nb−O−Mo symmetric vibrations, not seen in the IR spectra of binary molybdenum or niobium oxides. Earlier we

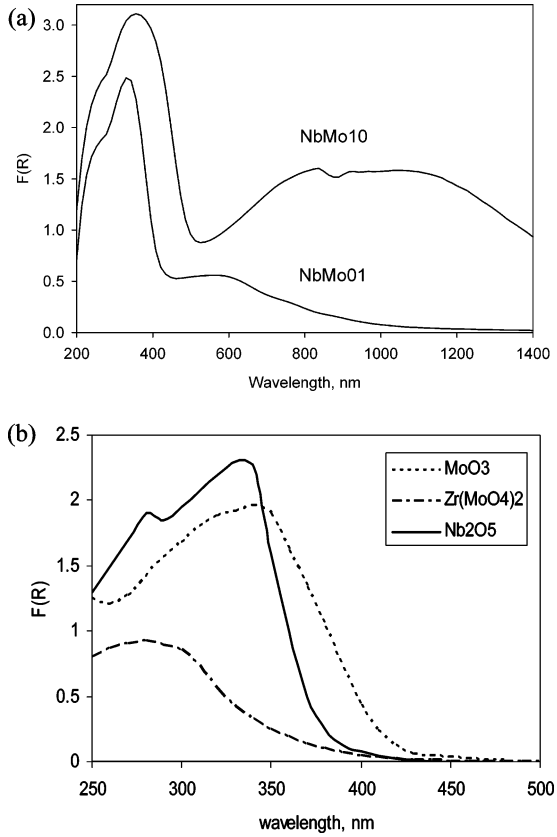

Figure 5. (a) UV−visible diffuse reflectance spectra of $Mo_3Nb_2O_{14}$ (NbMo10 solid) and $MoNb_6O_{18}$ (NbMo1 solid). The spectra are smoothed using a five-points algorithm. The feature at 860 nm is an artifact due to the detector change. (b) UV−visible spectra of the reference compounds (no absorption features observed above 500 for all oxides).

observed and similarly attributed the analogous band to the Zr−O−Mo systems.[12]

The infrared spectrum of $Mo_3Nb_2O_{14}$ can be compared with those previously reported for the Nb- and Ta-doped Mo_5O_{14} oxides.[13] The list of infrared bands is as follows: 950 sh, 905 (s), 875 (s), 825 (sh), 575 (w). The shoulder at ca. 750 cm^{-1} is also present in the spectrum of the Nb-doped sample but not discussed by the authors.

The UV−visible spectra were measured to clarify the origin of the intense coloration of the $Mo_3Nb_2O_{14}$ solid. The value of the band gap energy (E_g) was analyzed, and the eventual d−d transitions were looked for. We calculated the values of E_g for several relevant reference compounds as well.

In the UV−visible diffuse reflectance spectrum of $Mo_3Nb_2O_{14}$ there are two intense features corresponding respectively to the metal−oxygen charge transfer and to the d−d transitions (Figure 5). The absorption minimum separating these two bands is at 538 nm, in agreement with the green color of the solid. The high-energy (charge-transfer) band consists of two overlapping peaks, with the centers placed at 260 and 370 nm. The (d−d) feature is very broad and smears over the region 600−1400 nm. Its deconvolution to multiple individual peaks depends on the initial fit parameters and therefore is not reliable. For the niobium-rich mixed oxide $MoNb_6O_{18}$ the d−d feature has smaller intensity and is observed at higher energy. The value of E_g is also higher than that for $Mo_3Nb_2O_{14}$. The presence of the d−d transition in both Nb−Mo oxides suggests that the effect observed is not related to the unique structure of $Mo_3Nb_2O_{14}$ but seems to be rather a common property of the Nb−Mo oxides.

TABLE 2: Calculated Band Gap E_g vs Mean Electronegativity ME for the Nb−Mo Oxides and Some Reference Compounds

compd	$Mo_3Nb_2O_{14}$	$MoNb_6O_{18}$	Nb_2O_5	MoO_3	ZrO_2	$Zr(MoO_4)_2$	V_2O_5
E_g (eV)	2.35	3.05	3.4	3.0	4.9	4.1	2.3
ME	2.802	2.736	2.71	2.85	2.50	2.75	2.77
d(M−M)[a]	3.27	unknown	3.33	3.37	3.42	3.73	3.08

[a] The shortest metal−metal distance in the structure, Å.

Note that the intensity of UV−vis d−d transition bands (and visually observed color) for both Nb−Mo oxides are surprisingly constant whatever the preparation conditions. They are not affected by specimen quenching by immersion of hot solids in liquid nitrogen, neither by slight variations of composition of the reaction mixtures.

The values of optical gap E_g are listed in Table 2 for Nb−Mo oxides and several relevant compounds, i.e., binary oxides of Nb, Mo, and adjacent elements, as well as that of zirconium molybdate. For the reference compounds with the known band gap values, our measurements are in good agreement with the literature.[14−16]

Several reference compounds are included in Table 2 in order to check the general correlation between the E_g value and Pauling electronegativity of the constituents, provided they belong to the same type of oxides (d^0 nonmagnetic insulators). Indeed, charge transfer in the d^0 compounds is correlated to the ionization energies of the elements and by consequence to the mean electronegativity of the solids. Semiempirical correlations between the optical band gap of binary oxides and the difference of electronegativity between the oxygen and metallic elements (Pauling's extraionic energy) were proposed earlier,[17] as well as an extension of the correlation to the ternary oxides and hydroxides using the concept of average cationic or anionic group electronegativity.[18] One can expect that for the mixed d^0 oxides the value of E_g should be intermediate between the E_g values of the constituting oxides. Insulating d^0 oxides obey this general rule for rather different coordination of central atom. Indeed, the E_g averaging is observed for $Zr(MoO_4)_2$, composed of MoO_4 tetrahedra sharing corners with ZrO_6 octahedra.[19] This ternary oxide is derived from the reaction of binary oxides: MoO_3 composed by edge- and corner-sharing MoO_6 octahedra[20] and tetragonal ZrO_2 containing edge-sharing ZrO_8 cubes.[21] In chemical terms it can be speculated that the ease of reduction of the corresponding solids correlates with charge-transfer energy in them. The reaction between hardly reducible ZrO_2 and easily reducible MoO_3 leads to the solid with intermediate properties.

By contrast to the case of zirconium molybdate, the data of Table 2 indicate a significant decrease of the apparent E_g values for the $Mo_3Nb_2O_{14}$ oxide compared to the constituent binary oxides. Such a decrease may suggest the broadening of the conduction band due to the change of the solid structure, particularly due to the strong variations of the connectivity of metal oxygen polyhedra, because the last determines the conduction bandwidth. The progressive connection of metal−oxygen polyhedra leads to an increase in the interaction of metal d-orbitals through M−O−M bonds and therefore to the d-band widening which can be the cause of band gap decrease. However the qualitative comparison of the connectivity in $Mo_3Nb_2O_{14}$ with that of MoO_3 shows that the former structure has less edge sharing compared to the latter. Moreover the electonegativity of MoO_3 is higher, which should give even lower E_g, but the opposite is observed. It seems that not just the topological connectivity but metal−metal distances should be taken into account. The most important contribution to d-band broadening comes from the shortest M−O−M bonds; therefore the last are listed in Table 2 for comparison. Indeed, the V_2O_5 oxide which has the structure containing VO_6 octahedra sharing corners and edges,[22] has much lower E_g than MoO_3 although lower electronegativity. The essential difference between MoO_3 and V_2O_5 is that the last has much shorter metal−metal distance (Table 3). Similarly, somewhat decreased metal−metal distances are observed in $Mo_3Nb_2O_{14}$ compared to MoO_3. Obviously, both mean electronegativity and network connectivity should be considered to provide an adequate explanation of the observed E_g values. Thus, for example monotonic correlation (including $Mo_3Nb_2O_{14}$ oxide as a regular point) might be obtained if E_g is traced as a function of ratio of mean electronegativity to the shortest metal−metal distance (see Supporting Information). More detailed analysis of such semiempirical correlations is beyond the scope of this paper. Another probable explanation of the decreased E_g in Mo−Nb oxides is that some minor d^1 species are present, which have high extinction coefficients both in the charge-transfer and d−d transition regions.

TABLE 3: XPS Core Binding Energies of the Elements in $Mo_3Nb_2O_{14}$ and in the Binary Oxides

solid BE	$Mo_3Nb_2O_{14}$	Nb_2O_5	MoO_3
O 1s	530.9	530.70[a] (530.5)	531.30[b] (530.7)
Mo $3d_{5/2}$	232.8		233.0[b] (232.7)
Nb $3d_{5/2}$	207.1	207.3[a] (207.2)	

[a] Data from ref 36. [b] Data from ref 35.

A simple although low-precision probe of the mean electronic structure of an oxide is the XP spectroscopy. The core level binding energy may correlate with the electronic interaction and particularly with the oxygen partial charge.[23] As comparison of mixed oxide with the reference binary counterparts shows, the core binding energies of the elements in the mixed oxide and those of the precursor oxides are similar; the only significant difference being in the oxygen binding energies (Table 3, Figure 6), in agreement with the qualitative change of oxygen partial charge in the solids under study. The core level binding energies correspond to the highest oxidation states of the metals.[24] The metal surface contents in $Mo_3Nb_2O_{14}$ are in nearly perfect agreement with the solid stoichiometry (62.9% O, 15.4% Mo, 10.2% Nb; Mo/Nb atomic ratio 1.51; (Mo + Nb)/O atomic ratio 0.4), showing the absence of surface segregation phenomena. Carbon contamination (11.5% C) has the value usual for this type of experiments.

Although the lowest unoccupied orbitals cannot be detected by XPS technique (so the band gap values cannot be determined), it gives valuable information on the band positions. Indeed, the XPS spectra in the valent zone can be approximated as a result of convolution of the DOS below the Fermi level with a Gaussian−Lorentzian curve of approximately 2 eV width.[25] The spectra in the valence band regime of both individual oxides and the mixed one are presented in Figure 7. The lower energy band located at about 20−25 eV corresponds to the electrons of the O 2s level. The wide band at 0−10 eV corresponds to the O 2p nonbonding states and metal−oxygen molecular orbitals. Smaller features at lower energy are due to the weak covalent interactions between Mo 4d or Nb 4d and O 2p. The intensities at 0 eV and below are due to the instrumental noise. The binding energy of the O 2p states changes in the

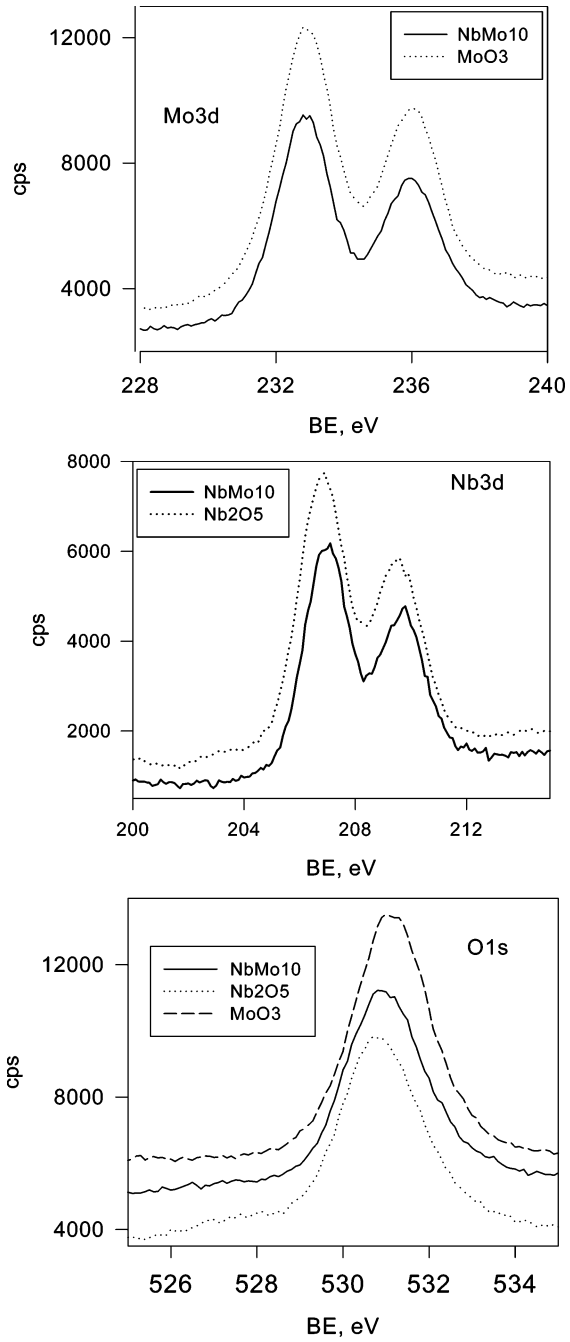

Figure 6. Core level XPS spectra of the elements in the NbMo10 specimen and in the parent binary oxides.

order Nb_2O_5 < $Mo_3Nb_2O_{14}$ < MoO_3. This is again in line with the variations of the mean electronegativity and the partial charge of oxygen in these compounds, which changes in the same sequence. The highest negative partial charge of oxygen in the Nb oxide corresponds as expected to its lower binding energy.

From the point of view of XPS characterization, the mixed oxide under study does not show any anomaly, demonstrating the intermediate properties between those of the corresponding binary oxides. Therefore the XP spectra corroborate the idea that the feature observed in the UV−vis spectra are due to some minority species rather than to modified electronic properties of the whole oxide structure.

A strong ESR signal of axial symmetry (Figure 8) was observed for all solids containing the $Mo_3Nb_2O_{14}$ phase. The spectra have axial symmetry, with $g_1 = 1.964$ and $g_2 = 1.898$,

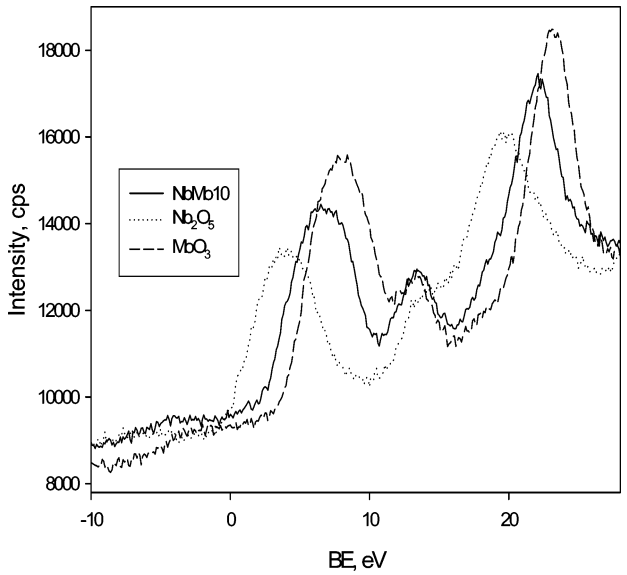

Figure 7. Valent band XPS spectra of $Mo_3Nb_2O_{14}$, MoO_3, and Nb_2O_5.

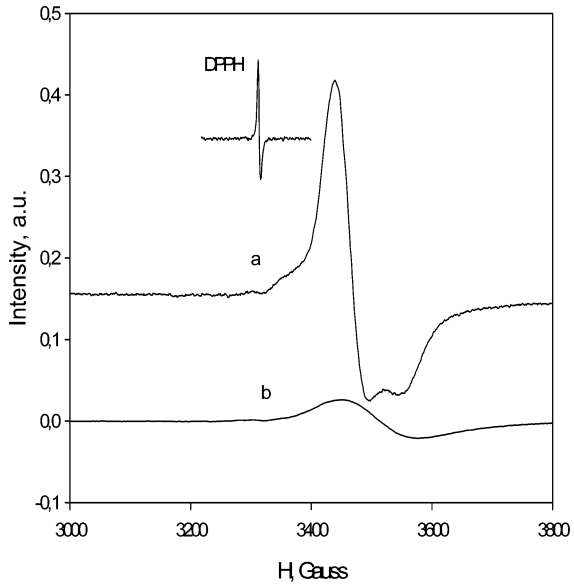

Figure 8. X-band, 9.312 GHz ESR spectra of $Mo_3Nb_2O_{14}$ (a) and $MoNb_6O_{18}$ (b) measured at 77 K.

the values being typical for six-coordinate d^1 species of Mo(V).[26−28] Comparison of the integrated intensity with that of the Varian pitch shows within the precision limits of this technique that in the solids under study nearly 0.8−1% of transition metal atoms are ESR-active. This quantity, being high on the ESR scale, could not be observed by the XPS technique. The niobium-rich sample (NbMo02) gives the spectrum of the same type but with an order of magnitude lower intensity, almost proportional to the decrease of molybdenum content. This corroborates the hypothesis that the molybdenum rather than niobium atoms are the carriers of the unpaired electrons.

The ESR spectra of NbMo07−NbMo10 solids were studied at variable temperatures. Only one axial signal was observed in all samples typical for the Mo(V) d^1 species in the distorted octahedral coordination.[28] The signal intensity is close in the samples NbMo07−NbMo10, which suggest that the presence of paramagnetic species is due to some equilibrium phenomenon and not caused by any deviations from the stoichiometry in the reaction mixtures. The signal intensity depends linearly on the $1/T$ value; the linear slope is similar for different samples (Figure

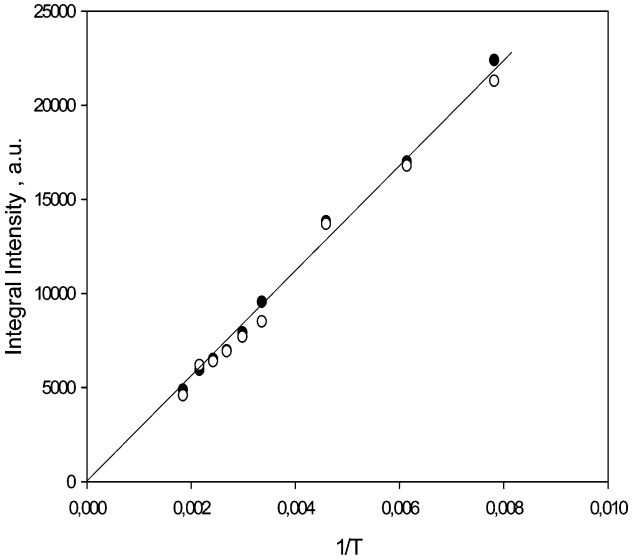

Figure 9. Temperature dependence of the ESR signal integrated intensity for NbMo07 (filled circles) and NbMo10 (open circles).

9). Since the signal intensity obeys the Curie law and the lines pass through the origin, we conclude that the paramagnetism is due to some diluted species with $S = {}^1/_2$. The number of such species is constant over the temperature range studied, and the spin−phonon interactions do not interfere significantly while the temperature increases; otherwise considerable deviations from the Curie law should be observed. (Note that the isostructural Mo_5O_{14} oxide is a weak Van Vleck paramagnetic,[29] in which the absence of temperature-dependent paramagnetic behavior excludes the occurrence of unpaired electrons on the distinct Mo(V) ions (probably, Mo(V) is completely involved in the Mo−Mo bonds in the edge-sharing polyhedra).

Quenching of the samples NbMo07−NbMo10 in liquid nitrogen after heating in sealed ESR ampules to 573−773 K does not lead to significant changes of the signal intensity. Note that neither the positions of the XRD peaks are changed within the NbMo07−NbMo10 series or as a result of specimens quenching. Therefore lattice parameters are not changed within this series. Moreover, the solid obtained by the instant immersion of hot reaction mixtures (1023 K) into liquid nitrogen (77 K) do not show any significant differences of the ESR signal compared to those obtained by exponential cooling.

The results of this study show clearly that stable and abundant Mo(V) species are formed in the $3MoO_3{\cdot}Nb_2O_5$ solid during its preparation in open air or in sealed ampules. However the origin of the effect is not clear, and several questions arise. Why do the mixed oxides show this property, whereas the corresponding binary oxides do not demonstrate the formation of paramagnetic centers under the same conditions? Why is the effect so astonishingly preparation-independent? Molybdenum oxide is relatively easy to reduce, but it does not show any paramagnetic centers upon firing in air. As with niobium oxide, its reduction is more difficult than that of MoO_3. Moreover, large numbers of main and transition group molybdates and niobates exist, which do not show any similar effect, remaining purely d^0 compounds (e.g. Zr and Al molybdates do not show any paramagnetism when heated in air, in the range of temperatures from ambient to 1273 K).[30,31] Some mixed oxides of main and transition metal compounds (V, Bi) show reversible redox behavior in air, absorbing and releasing oxygen, but always demonstrate very strong influence of preparation and treatments on the metals reduction state.[32] This is certainly not the case for the systems under study, since no oxygen release was observed by mass spectroscopy during the heating of the oxide mixtures from room temperature up to 1273 K (not shown). Therefore, the presence of paramagnetic centers seems to be an immanent property of the solids under study.

As resumed below, the most important findings requiring a coherent explanation are as follows:

(1) The presence of both niobium and molybdenum is necessary for the formation of d^1 species.

(2) The effect is certainly not related to the unique structure of Mo_5O_{14} adopted by the $Mo_3Nb_2O_{14}$ oxide but seems to be characteristic of the simultaneous presence of Mo and Nb within any ingenious 3-D crystalline structure, since the niobium-rich oxide $MoNb_6O_{18}$ also shows coloration and paramagnetic centers, though to a lesser extent.

(3) The number of paramagnetic species and the intensity of color do not depend on slight deviations from stoichiometry. The paramagnetic species cannot be annealed, neither are they sensible to the quenching of the solids. Rather, they are self-generated by the structure and preserve their number at least in the range of temperatures of 77−523 K.

These findings lead to the conclusion that the paramagnetic centers are formed within the solid bulk during the preparation (973−1023 K) due to substitution disorder in the crystalline structure. Probably, a Boltzmann distribution of Nb and Mo is achieved within the crystal sites at high preparation temperature and, due to the similarity of metal mass and properties, leads to an important degree of occupation of Nb sites by Mo. The next question arises; why do the Mo atoms occupying the Nb crystallographic sites create any redox rearrangement?

As a working hypothesis, we suppose that configurations are unstable in which μ_3 oxygens are bonded to three Mo(VI) atoms. Presumably, these are particularly the O15 atoms of the structure (Figure 3), which have almost symmetrical O−M bond lengths at 2.019, 2.041, and 2.046 Å. Speaking in simple chemical terms, when Nb(V) is replaced by the more electronegative Mo(VI), the configuration containing μ_3 oxygen becomes unstable and one oxygen ion is oxidized, leading to a hole in the valence band, whereas one of Mo(VI) atoms is reduced, as formally expressed by eq 1.

$$Mo^{6+}{}_{Nb} + O^{2-} \rightleftharpoons Mo^{5+}{}_{Nb} + O^{-} \qquad (1)$$

This redox disproportionation occurs only in the all-molybdenum configurations, since Mo(VI) is stronger second-order Jann−Teller (SOJT) distorder and stronger oxidizer than Nb(V). Note that in the layered MoO_3 structure only μ_1 and μ_2 oxygen is present. At the same time, formation of shear planes in the reduced Mo oxides includes formation of μ_3 oxygen. To verify the validity of this model, further advanced characterizations and electronic structure calculations are planned for this system. Otherwise, if the proposed hypothesis is true, other 3-D oxides with substitutional disorder can be looked for, in which the instability of μ_3 oxygen will produce self-generated reduced centers. Other couples of elements can be tried, containing stronger (V, Mo, Cr) and weaker (W, Nb, Ta) oxidants and SOJT distorders.

Conclusion

In the present work, the mixed oxide $Mo_3Nb_2O_{14}$ was synthesized and characterized. The structure of this solid as refined by the Rietveld technique is similar to that of the binary oxide Mo_5O_{14}, eminently important for catalysis.[33,34] Although according to chemical analysis data and XPS spectroscopy, both metals are mostly in their highest oxidation states; the solid

possess an intense d^1 absorption band in the UV−visible spectrum as well as a high amount of paramagnetic centers. Both the intensity of the absorption band in the optical spectrum and the ESR signal are independent of the preparation details, being rather the characteristics of each individual compound. The mechanism of the genesis of the reduced centers is presumably based on a substitution disorder between Nb and Mo atoms. The coordination state of the reduced centers as well as the relationship between the electronic structure of this oxide and its properties are under study.

Supporting Information Available: Tables showing full chemical analysis data for the specimens prepared, final atomic fractional coordinates, and B_{iso} values obtained by Rietveld refinement for NbMo10, cell refinement fit parameters for NbMo10, general Rietveld fit parameters for NbMo10, and selected bond lengths and angles in the refined $Mo_3Nb_2O_{14}$ structure and figures showing the instrumental line width for the Bruker XRD device used, fragments of the XRD pattern of NbMo10 in the low-angle and middle-angle regions, the XRD pattern of NbMo01, and the optical gap for solids as a function of the ratio of E_{mean} to the shortest metal−metal distance. This material is available free of charge via the Internet at http://pubs.acs.org.

References and Notes

(1) Knobl, S.; Zenkovets, G. A.; Kryukova, G. N.; Ovsitser, O.; Niemeyer, D.; Schlögl, R.; Mestl, G. *J. Catal.* **2003**, *215*, 177.
(2) Botella, P.; García-González, E.; Dejoz, A.; López Nieto, J. M.; Vázquez, M. I.; González-Calbet, J. *J. Catal.* **2004**, *225*, 428.
(3) Afanasiev, P.; Fischer, L.; Beauchesne, F.; Danot, M.; Gaborit, V.; Breysse, M. *Catal. Lett.* **2000**, *64*, 59.
(4) ICSD Inorganic Crystal Structure Database (ICSD). CD-ROM, version 2004, FIZ Karlsruhe, Fachinformationszentrum Karlsruhe: Eggenstein-Leopoldshafen, Germany.
(5) Rodriguez-Carvajal, J. *Physica B* **1993**, *192*, 55.
(6) Kraus, W.; Nolze, G. *J. Appl. Crystallogr.* **1996**, *29*, 301.
(7) Werner, P. E.; Eriksson, L.; Westdahl, M. *J. Appl. Crystallogr.* **1985**, *18*, 367.
(8) Louer, D. Dicvol Program, Groupe de Cristallochimie, Université de Rennes, I, Rennes Cedex, France.
(9) Weber, R. S. *J. Catal.* **1995**, *151*, 470.
(10) Kihlborg, L. *Ark. Kemi* **1963**, *21*, 427.
(11) Kihlborg, L. *Acta Chem. Scand.* **1969**, *23*, 1834.
(12) Afanasiev, P.; Geantet, C.; Breysse, M.; Coudurier, G.; Vedrine, J. C. *J. Chem. Soc., Faraday Trans.* **1994**, *90*, 193.
(13) Cariati, F.; Bart, J. C. J.; Sgamellotti, A. *Inorg. Chim. Acta* **1981**, *48*, 97.
(14) Hoppmann, G.; Salje, E. *Opt. Commun.* **1979**, *30*, 199.
(15) Dimitrov, V.; Sakka, S. *J. Appl. Phys.* **1996**, *79*, 1736.
(16) Conlon, D. C.; Doyle, W. P. *J. Chem. Phys.* **1961**, *35*, 752.
(17) Portier, J.; Campet, G.; Kwon, C. W.; Etourneau, J.; Subramanian, M. A. *Int. J. Inorg. Mater.* **2001**, *3*, 1091.
(18) Di Quarto, F.; Sunseri, C.; Piazza, S.; Romano, M. C. *J. Phys. Chem. B* **1997**, *101*, 2519.
(19) Serezhkin, V. N.; Efremov, V. A.; Trunov, V. K. *Russ. J. Inorg. Chem.* **1987**, *32*, 1566.
(20) Andersson, G.; Magneli, A. *Acta Chem. Scand.* **1950**, *4*, 793.
(21) Barker, W. W.; Bailey, F. P.; Garrett, W. *J. Solid. State Chem* **1973**, *7*, 448.
(22) Bachmann, H. G.; Ahmed, F. R.; Barnez, W. H. *Z. Kristallogr.* **1961**, *115*, 110.
(23) Delamar, M. *J. Electron Spectrosc. Relat. Phenom.* **1990**, *53*, C11.
(24) Moulder, F.; Stickle, W. F.; Sobol, P. E.; Bomben, K. D. *Handbook of XPS*; Perkin-Elmer Corp.: Eden Prairie, MN, 1992.
(25) Hixson, H.; Sherwood, P. M. *Chem. Mater.* **1996**, *8*, 2643.
(26) Sojka, Z.; Adamski, A.; Che, M. *J. Mol. Catal.* **1996**, *112*, 469.
(27) Louis, C.; Che, M.; Anpo, M. *J. Catal.* **1993**, *141*, 453.
(28) Che, M.; Sojka, Z. *Top. Catal.* **2001**, *15*, 2.
(29) Ekström, T. *Acta Chem. Scand.* **1972**, *26*, 3381.
(30) Lind, C.; Wilkinson, A. P.; Hu, Z.; Short, S.; Jorgensen, J. D. *Chem. Mater.* **1998**, *10*, 2335.
(31) Forzatti, P.; Mari C. M.; Villa, C. *Mater. Res. Bull.* **1987**, *22*, 1593.
(32) Abrahams, I.; Bush, A. J.; Krok, F.; Hawkes, G. E.; Sales, K. D.; Thornton, P.; Bogusz, W. *J. Mater. Chem.* **1998**, *8*, 1213.
(33) Dieterle, M.; Mestl, G.; Jäger, G.; Uchida, Y.; Hibst H.; Schlögl, R. *J. Mol. Catal. A* **2001**, *174*, 169.
(34) Mestl, G. Linsmeier, Ch.; Gottschall, R.; Dieterle, M.; Find, J.; Herein, D.; Jäger, J.; Uchida, Y.; Schlögl, R. *J. Mol. Catal. A* **2000**, *162*, 463.
(35) Kim, G.-T.; Park, T.-K.; Chung, H.; Kim, Y.-T.; Kwon, M.-H.; Choi, J.-G. *Appl. Surf. Sci.* **1999**, *152*, 35.
(36) Barreto, O. T.; Buyuklimanli, T.; Lampert, C. M. *Solar Energy Mater. Solar Cell* **1995**, *36*, 433.